An observer looks at the cell temperature in automotive battery packs

Maxime Debert, Guillaume Colin, Gérard Bloch, Yann Chamaillard

An observer looks at the cell temperature in automotive battery packs

Maxime Debert[a], Guillaume Colin[b,*], Gérard Bloch[c], Yann Chamaillard[b]

[a] *Renault SAS, France, maxime.debert@renault.com*
[b] *Laboratoire PRISME, Université d'Orléans, France, {guillaume.colin,yann.chamaillard}@univ-orleans.fr*
[c] *Centre de Recherche en Automatique de Nancy (CRAN), Université de Lorraine, CNRS, France, gerard.bloch@univ-lorraine.fr*

Abstract

The internal temperature of Li-ion batteries for electric or hybrid vehicles is an important factor influencing their ageing. Generally not measured, it can be reconstructed from an external measurement and a model. This paper presents the simplified modelling of heat transfers in a battery module, leading to a Linear Parameter-Varying (LPV) model. Then, a polytopic observer is proposed to estimate the cell temperature and internal resistance, ensuring a tradeoff between the convergence speed and the noise of the estimated states. Experimental results show the good quality of the estimation and the diagnosis potential offered by internal resistance reconstruction.

Keywords: Li-ion battery, Electric Vehicle (EV), Plug-in Hybrid Electric Vehicle (PHEV), Thermal modelling, Temperature estimation, Internal resistance estimation, Linear Parameter-Varying (LPV) system, Polytopic observer

1. Introduction

The battery is the keystone of Electric Vehicles (EV) and Plug-in Hybrid Electric Vehicles (PHEV), which require electric traction over extended periods in charge-depleting mode. It is a heavy, bulky, and costly device, which constitutes the main obstacle to the mass distribution of such vehicles. Moreover, the lifetime of a current battery is shorter than that of the car. Improving the battery ageing is certainly the key to the durability of the whole vehicle.

The ageing process of Li-ion batteries is highly complex and affected by many factors: internal temperature, use, calendar life (even unused, a battery loses little by little its capacity over time (Ratnakumar et al., 1999), state of charge (SOC), depth of discharge/charge (DOD/DOC), etc. Amongst the parameters influencing the performance degradation of such batteries, the internal temperature is known to be one of the most important (Broussely et al., 2005; Vetter et al., 2005). However, in general, due to the cost and manufacturing process, the internal temperature cannot be measured, neither at the core of the reactions nor close to the battery cells.

The Li-ion battery pack studied in this work is made up of numerous modules, and these modules are in turn composed of several prismatic cells. The battery temperature is measured in the vehicles by a thermistor mounted in an interstice of an equipped module. The measurement gives therefore an image of the temperature of the air trapped in the module, and the information about the cell temperature is smoothed and delayed. The reduction can reach tens of degrees, with very long time delays, leading to very conservative strategies of power limitation. Moreover, this means that the internal parameters, which vary according to the internal temperature, cannot be properly estimated.

It is therefore necessary to estimate the temperature as close as possible to the cell. To this end, the temperature and internal resistance of the cell can be reconstructed from the external measurement given at the module level, by using a thermal model. A similar approach was proposed to estimate the SOC in Hu et al. (2009) and Hu and Yurkovich (2012). Lin et al. (2013) propose an adaptive observer of the core temperature of a cylindrical lithium ion battery which permits to deduce the internal resistance. In particular, monitoring the internal resistance of the battery would make it possible to develop diagnosis functions (Hall et al., 2005). In this paper the estimation of internal resistance is used for monitoring the battery safety by detecting abnormal conditions.

The rest of the paper is organized as follows. Section 2 presents the control-oriented modelling of heat transfers in a battery module, leading to a Linear Parameter-Varying (LPV) model. Then, a so-called polytopic observer, with guaranteed convergence, is proposed in Section 3 to estimate the cell temperature and internal resistance. An approach to limit the amplification of the measurement noise for high observer gains is developed. Some results obtained from a specially instrumented module are illustrated in Section 4, showing the good quality of the estimation and the ease of use for real-time implementation.

The main contributions of the paper are twofold: a generic approach for the design of an observer for LPV systems ensuring both the convergence of the estimation and a tradeoff between the convergence speed and the noise of the estimated

*Corresponding author.

states; the estimation of Li-ion battery internal resistance and temperature, simple to implement and built for on board diagnosis of batteries for electric or hybrid vehicles.

2. Thermal model

2.1. Physical model

For the design of the cell temperature observer, a control-oriented but representative model has to be built. In our case, the battery module contains several prismatic cells and the model differs from the one of Lin et al. (2013), which considers a cylindrical battery. The main assumptions of the proposed zero-dimensional model are that the cells have the same uniform temperature (this has been checked from measurements) and exchange heat with the air trapped in the module by natural convection. A thermistor, used in mass-produced vehicles, measures this air temperature. The module is cooled down by convection, forced or not, depending on the cooling mode of the battery pack.

The thermal model of the battery module is based on the physical equations of heat flow balance using equivalent thermal resistances (Pesaran, 2002; Guzzella and Sciarretta, 2007; Debert et al., 2008; Forgez et al., 2010; Muratori et al., 2010; Lin et al., 2012). The heat transfers are presented in Fig. 1, where four temperatures are considered: the cell temperature T_{cell}, the one given by the sensor T_{sens}, the temperature of the cooled wall (casing) T_{cas} and the temperature of the air cooling the module T_{air}. The difference between the cell edge and core temperatures does not justify another state (confirm by the fact that the Biot number is small).

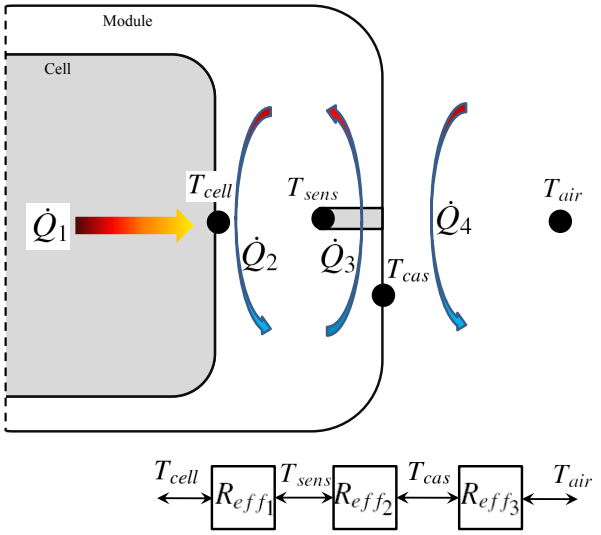

Figure 1: Heat flow transfers and equivalent resistance modelling.

The temperatures are in K, heat flows in W=J/s and thermal resistances in K/W. At the first node, the temperature T_{cell} is given by integrating the difference between the heat flows produced $\dot{Q}_1$ and lost $\dot{Q}_2$:

$$T_{cell} = \int_0^t \frac{\dot{Q}_1 - \dot{Q}_2}{C_{V_1}} dt, \tag{1}$$

where C_{V_1} the heat capacity at constant volume (J/K) of the cell. The heat flow $\dot{Q}_1$ is produced by the Joule effect and chemical reaction:

$$\dot{Q}_1 = RI_{bat}^2 + T_{cell}\Delta S \frac{1}{nF}, \tag{2}$$

with R the cell internal resistance (Ω), I_{bat} the charge/discharge current of the battery (A), ΔS the entropy change of the cell reaction, n the number of electrons exchanged and F the Faraday's constant. However, as shown in Williford et al. (2009) and confirmed by our experiments, the chemical contribution ΔS can be neglected for the considered chemistry, so that

$$\dot{Q}_1 \approx RI_{bat}^2. \tag{3}$$

The heat flow $\dot{Q}_2$ lost by the cell is caused by the convection of the air trapped inside the module:

$$\dot{Q}_2 = \frac{T_{cell} - T_{sens}}{R_{eff_1}}, \tag{4}$$

where $R_{eff_1} = \frac{1}{h_1 A_1}$ is a thermal resistance, with A_1 the area (m^2) swept by the cooling air and h_1 the heat transfer coefficient ($W/m^2/K$).

At the second node, the temperature measured by the sensor T_{sens} is in turn modelled by:

$$T_{sens} = \int_0^t \frac{\dot{Q}_2 - \dot{Q}_3}{C_{V_2}} dt, \tag{5}$$

with C_{V_2} the heat capacity at constant volume (J/K) of the air trapped inside the module, and where again the heat flow $\dot{Q}_3$ is expressed from a thermal resistance:

$$\dot{Q}_3 = \frac{T_{sens} - T_{cas}}{R_{eff_2}}. \tag{6}$$

Finally at the third node, the casing temperature T_{cas} is obtained with the same approach:

$$T_{cas} = \int_0^t \frac{\dot{Q}_3 - \dot{Q}_4}{C_{p_3}} dt, \tag{7}$$

where C_{p_3} is the heat capacity at constant pressure (J/K) of the external air, and where

$$\dot{Q}_4 = \frac{T_{cas} - T_{air}}{R_{eff_3}}. \tag{8}$$

The temperature of the air cooling the module T_{air} is given by the cooling system and the thermal resistance R_{eff_3} differs depending on the cooling mode (convection forced or not).

2.2. State space model

It is known that the internal resistance is influenced by many factors as the SOC, temperature or sign of the current. For the sake of estimator design, it is assumed that battery internal resistance variations are rather slow for a wide range of battery operating conditions, because SOC and battery temperature are typically slowly-changing as well. When the battery is nearly fully charged or deeply discharged, these variations tend to be

much more emphasized. However, these operating conditions are not likely to occur, because the battery management system needs to prevent them beforehand. On the other hand, detecting abnormal battery state from the estimated internal resistance is also aimed. Therefore, in order to avoid the non detection of an abnormal situation due to an incorrect value of a parameter like SOC, temperature, cell voltage, the cell internal resistance R is simply assumed to vary slowly. This simplification has been also proposed in Plett (2004) for estimating the State Of Health (SOH) with a Kalman filter. However, if necessary, a more complex model could be used for the internal resistance. Thus, finally the thermal model can be written as a state space model

$$\left\{\begin{array}{lcl} \dot{T}_{cell} &=& k_1\left(RI_{bat}^2 - k_4\left(T_{cell} - T_{sens}\right)\right) \\ \dot{T}_{sens} &=& k_2\left(k_4\left(T_{cell} - T_{sens}\right) - k_5\left(T_{sens} - T_{cas}\right)\right) \\ \dot{T}_{cas} &=& k_3\left(k_5\left(T_{sens} - T_{cas}\right) - k_6\left(T_{cas} - T_{air}\right)\right) \\ \dot{R} &=& 0, \end{array}\right. \tag{9}$$

with the parameters

$$\left\{\begin{array}{lll} k_1 = \frac{1}{C_{V_1}}, & k_2 = \frac{1}{C_{V_2}}, & k_3 = \frac{1}{C_{P_3}}, \\ k_4 = \frac{1}{R_{eff_1}}, & k_5 = \frac{1}{R_{eff_2}}, & k_6 = \frac{1}{R_{eff_3}}. \end{array}\right. \tag{10}$$

These parameters, assumed to be constant because of the temperature variation considered, can be theoretically calculated, e.g. from Nusselt numbers (Cheron, 1999). They will be identified here from experiments, as presented below in Section 2.3.

Defining the system state vector, input and output respectively as $\mathbf{x} = [T_{cell}\ T_{sens}\ T_{cas}\ R]^T$, $u = T_{air}$ and $y = T_{cell}$, a Linear Parameter-Varying (LPV) model in continuous time t:

$$\left\{\begin{array}{l} \dot{\mathbf{x}}(t) = \mathbf{A_c}(\rho(t))\mathbf{x}(t) + \mathbf{b_c}u(t) \\ y(t) = \mathbf{c}\mathbf{x}(t) \end{array}\right. \tag{11}$$

can be written, with

$$\mathbf{A_c}(\rho(t)) = \begin{bmatrix} -k_1k_4 & k_1k_4 & 0 & k_1I_{bat}^2(t) \\ k_2k_4 & -k_2(k_4+k_5) & k_2k_5 & 0 \\ 0 & k_3k_5 & -k_3(k_5+k_6) & 0 \\ 0 & 0 & 0 & 0 \end{bmatrix}, \tag{12}$$

$$\mathbf{b_c} = \begin{bmatrix} 0 \\ 0 \\ k_3k_6 \\ 0 \end{bmatrix}, \mathbf{c} = \begin{bmatrix} 0 & 1 & 0 & 0 \end{bmatrix}, \tag{13}$$

where the varying parameter $\rho(t) = I_{bat}^2(t)$ is available because the current of battery charge or discharge I_{bat} is measured.

Approximating $\dot{\mathbf{x}}(t)$ by $(\mathbf{x}_{k+1} - \mathbf{x}_k)/t_s$, with the sampling period t_s, a discrete-time model is finally obtained:

$$\left\{\begin{array}{l} \mathbf{x}_{k+1} = \mathbf{A}(\rho_k)\mathbf{x}_k + \mathbf{b}u_k \\ y_k = \mathbf{c}\mathbf{x}_k, \end{array}\right. \tag{14}$$

with $\mathbf{A} = I + t_s\mathbf{A_c}$ and $\mathbf{b} = t_s\mathbf{b_c}$.

2.3. Parameter identification

For the parameter identification of the proposed thermal model (14), an experimental module was introduced in a battery pack. This module, shown in Fig. 2, is instrumented with a thermocouple placed between the most internal cells (in red, giving T_{cell}), the mass production temperature sensor (in green, giving T_{sens}), and a thermocouple placed on the casing (in blue, giving T_{cas}). A cycle of battery use was carried out, with a charge followed by a typical Electric Vehicle (EV) charge depleting. The gathered data have been divided in two parts, an identification set only used for parameter estimation and a validation set for model testing. The parameters were identified by

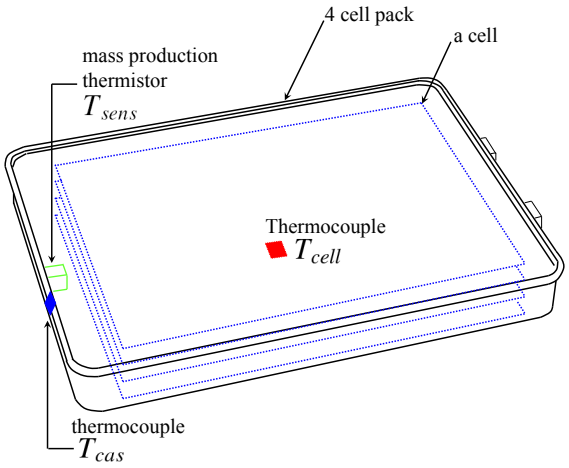

Figure 2: Specially equipped module for parameter identification.

a Nelder-Mead simplex (direct search) algorithm minimizing the Root Mean Squared Errors (RSME) between the predicted and measured values, giving $k_1 = 0.0008, k_2 = 0.4657, k_3 = 0.0041, k_4 = 1.1461, k_5 = 3.8434, k_6 = 0.3801$. Several initialisations have been performed to ensure satisfactory convergence. For a sampling period $t_s = 0.1$ s, this leads for system (14) to the following matrices

$$\mathbf{A} = \begin{bmatrix} 0.999908 & 9.169e^{-4} & 0 & 8e^{-4}I_{bat}^2(k) \\ 0.533738 & 0.767638 & 1.78987 & 0 \\ 0 & 0.01575 & 0.998268 & 0 \\ 0 & 0 & 0 & 1 \end{bmatrix}, \tag{15}$$

$$\mathbf{b} = \begin{bmatrix} 0 \\ 0 \\ 1.5584e^{-4} \\ 0 \end{bmatrix}, \mathbf{c} = \begin{bmatrix} 0 & 1 & 0 & 0 \end{bmatrix}. \tag{16}$$

Data and estimation results are shown in Fig. 3. The model is then simulated on the validation data as shown in Fig. 4. It is worth noting that the simulation is a N-step ahead prediction based only on the battery current, included in the time-varying parameter, and constant air external temperature T_{air}. Table 1 shows the Root Mean Squared Error and the correlation coefficient for the estimation of the three temperatures T_{cell}, T_{sens} and T_{cas} on the identification data and on the validation data. The model gives quite good results on the identification data. On

the validation data, the errors are bigger but the dynamics are respected. Therefore a (closed loop) observer is necessary to compensate these estimation errors and accomodate the ageing and parameter dispersion of batteries.

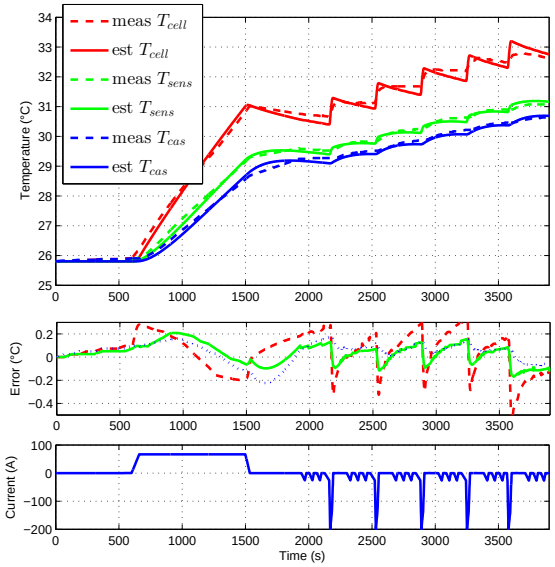

Figure 3: Identification of the thermal model.

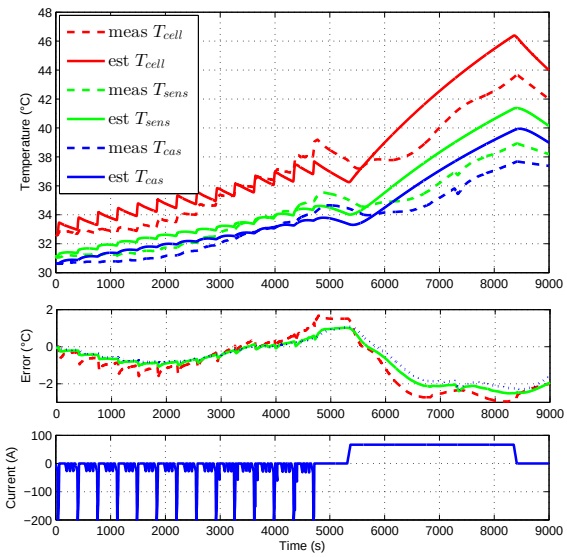

Figure 4: Validation of the thermal model.

3. Observer for LPV system

This section is devoted to the design of an observer for system (14), with guaranteed convergence while limiting the effect of the noise measurement on the reconstructed state.

Table 1: Root Mean Squared Error (RMSE) and correlation coefficient with the thermal model for the estimation of the three temperatures T_{cell}, T_{sens} and T_{cas}.

Data	Temperature	RMSE (°C)	Corr. coef.
Identification	T_{cell}	0.17	0.998
	T_{sens}	0.10	0.999
	T_{cas}	0.10	0.999
Validation	T_{cell}	1.6	0.959
	T_{sens}	1.3	0.961
	T_{cas}	1.2	0.957

3.1. Principle

Consider the discrete time Linear Parameter-Varying (LPV) system subject to measurement noise

$$\begin{cases} \mathbf{x}_{k+1} = \mathbf{A}(\boldsymbol{\rho}_k)\mathbf{x}_k + \mathbf{B}\mathbf{u}_k \\ \mathbf{y}_k = \mathbf{C}\mathbf{x}_k + \mathbf{D}\mathbf{v}_k \end{cases} \tag{17}$$

where $\mathbf{x}_k \in \mathbb{R}^n$, $\mathbf{u}_k \in \mathbb{R}^p$, $\mathbf{y}_k \in \mathbb{R}^m$ are respectively the state, input and output vectors of the system, $\mathbf{v}_k \in \mathbb{R}^q$ the zero-mean measurement noise, and $\boldsymbol{\rho}_k$ a measurable time varying parameter vector.

As $\boldsymbol{\rho}_k$ is bounded, it evolves in a compact set and can always be included in a convex polytope $\mathcal{D}_\rho$. Hence, $\boldsymbol{\rho}_k$ admits the polytopic decomposition

$$\boldsymbol{\rho}_k = \sum_{i=1}^{N} \boldsymbol{\xi}_k^i \boldsymbol{\theta}_i, \tag{18}$$

where the vector $\boldsymbol{\xi}_k = [\boldsymbol{\xi}_k^1 \dots \boldsymbol{\xi}_k^N]^T$ belongs to the convex set $S = \{\boldsymbol{\xi}_k \in \mathbb{R}^N, \boldsymbol{\xi}_k^i \geq 0 \ \forall i, \sum_{i=1}^N \boldsymbol{\xi}_k^i = 1\}$. The constant vectors $\boldsymbol{\theta}_i, \dots, \boldsymbol{\theta}_N$ are the N vertices of the convex polytope $\mathcal{D}_\rho$. Note that, at each time k, $\boldsymbol{\xi}_k$ depends on the available time-varying parameter $\boldsymbol{\rho}_k$. It will be noted $\boldsymbol{\xi}_k(\boldsymbol{\rho}_k)$ to recall this dependence.

Then, as the state matrix $\mathbf{A}(\boldsymbol{\rho}_k)$ for LPV systems depends linearly on $\boldsymbol{\rho}_k$, it can be rewritten in a polytopic form (Millérioux et al., 2005; Halimi et al., 2013) as

$$\mathbf{A}(\boldsymbol{\rho}_k) = \sum_{i=1}^{N} \xi_k^i(\boldsymbol{\rho}_k)\mathbf{A_i}. \tag{19}$$

The constant matrices $\mathbf{A}_i$, $i = 1, \cdots, N$, are the vertices of the convex hull $\mathcal{D}_A$ including the compact set where $\mathbf{A}(\boldsymbol{\rho}_k)$ evolves.

The state reconstruction for system (17) can be achieved by a so-called polytopic observer

$$\begin{cases} \hat{\mathbf{x}}_{k+1} = \mathbf{A}(\boldsymbol{\rho}_k)\hat{\mathbf{x}}_k + \mathbf{B}\mathbf{u}_k + \mathbf{K}(\boldsymbol{\rho}_k)(\mathbf{y}_k - \hat{\mathbf{y}}_k) \\ \hat{\mathbf{y}}_k = \mathbf{C}\hat{\mathbf{x}}_k \end{cases}, \tag{20}$$

where the observer gain can be time varying, i.e. $\mathbf{K}(\boldsymbol{\rho}_k) = \sum_{i=1}^{N} \boldsymbol{\xi}_k^i(\boldsymbol{\rho}_k)\mathbf{K}_i$, or constant, i.e. $\mathbf{K}(\boldsymbol{\rho}_k) = \mathbf{K}$, which is simpler for further use, but will constrain the LMIs to be solved.

From (17), (20) and (19), it can be shown that the state reconstruction error $\boldsymbol{\epsilon}_k = \mathbf{x}_k - \hat{\mathbf{x}}_k$ is governed by

$$\boldsymbol{\epsilon}_{k+1} = \mathcal{A}(\boldsymbol{\rho}_k)\boldsymbol{\epsilon}_k - \mathbf{K}(\boldsymbol{\rho}_k)\mathbf{D}\mathbf{v}_k. \tag{21}$$

where $\mathcal{A}(\boldsymbol{\rho}_k) = \sum_{i=1}^{N} \boldsymbol{\xi}_k^i(\boldsymbol{\rho}_k)(\mathbf{A}_i - \mathbf{K}_i\mathbf{C})$, with $\mathbf{K}_i = \mathbf{K}$ for constant gain.

Consider first the noise free case, i.e. $\mathbf{v}_k = 0$ and

$$\boldsymbol{\epsilon}_{k+1} = \mathcal{A}(\boldsymbol{\rho}_k)\boldsymbol{\epsilon}_k. \tag{22}$$

The conditions of global convergence toward zero of the state reconstruction error (22) are ensured from the following Theorem (Millérioux et al., 2004).

Theorem 1. *The global convergence of* (22) *is achieved whenever the following set of Linear Matrix Inequalities*

$$\begin{bmatrix} \mathbf{P}_i & \mathbf{A}_i^T\mathbf{G}_i^T - \mathbf{C}^T\mathbf{F}_i^T \\ \mathbf{G}_i\mathbf{A}_i - \mathbf{F}_i\mathbf{C} & \mathbf{G}_i + \mathbf{G}_i^T - \mathbf{P}_j \end{bmatrix} > 0 \tag{23}$$

where the positive-definite matrices $\mathbf{P}_i$*, the matrices* $\mathbf{F}_i$ *and* $\mathbf{G}_i$ *are unknown, is feasible for all* $(i, j) \in \{1, \ldots, N\} \times \{1, \ldots, N\}$.

The matrices $\mathbf{F}_i$ and $\mathbf{G}_i$ are determined when solving (23) by convex optimization.

Consider now noisy measurements, i.e. $\mathbf{v}_k \neq 0$. Although the stability of the state reconstruction error is ensured by Theorem 1, high gain values which can be obtained by solving the LMIs (23) can lead to unusable estimated states. Indeed, as can be seen in (21), the observer gain $\mathbf{K}$ also acts on the measurement noise. Thus, there is a need to balance the speed of convergence and the influence of measurement noise.

To this end, let us define the upper bound σ of the $\mathcal{L}_2$ gain as a scalar verifying:

$$\sup_{\|\mathbf{v}\|_2 \neq 0} \frac{\|\mathbf{z}\|_2}{\|\mathbf{v}\|_2} < \sigma \tag{24}$$

where $\mathbf{z}_k = \tilde{\mathbf{C}}\boldsymbol{\epsilon}_k$. Considering $\mathbf{z}_k$ instead of $\boldsymbol{\epsilon}_k$ directly allows for instance to select particular reconstructed states through $\tilde{C}$. The following Theorem 2 can thus be stated, with a proof, based on (Millérioux and Daafouz, 2006), given in the appendix.

Theorem 2. *The global convergence of* (21)*, with* $\mathbf{v}_k \neq 0$ *and the constraint* (24)*, is ensured if there exist symmetric matrices* $\mathbf{P}_i$ *and matrices* $\mathbf{G}_i$ *and* $\mathbf{F}_i$ *such that, for* $(i, j) \in \{1 \ldots N\} \times \{1 \ldots N\}$*, the following matrix inequalities are feasible*

$$\begin{bmatrix} \mathbf{P}_i & \mathbf{0} & (\mathbf{G}_i\mathbf{A}_i - \mathbf{F}_i\mathbf{C})^T & \tilde{\mathbf{C}}^T \\ \mathbf{0} & \sigma\mathbf{1} & (-\mathbf{F}_i\mathbf{D})^T & \mathbf{0} \\ \mathbf{G}_i\mathbf{A}_i - \mathbf{F}_i\mathbf{C} & -\mathbf{F}_i\mathbf{D} & \mathbf{G}_i + \mathbf{G}_i^T - \mathbf{P}_j & \mathbf{0} \\ \tilde{\mathbf{C}} & \mathbf{0} & \mathbf{0} & \sigma\mathbf{1} \end{bmatrix} > 0. \tag{25}$$

For both noise free and noisy cases, the time varying observer gain is given by

$$\mathbf{K}(\boldsymbol{\rho}_k) = \sum_{i=1}^{N} \boldsymbol{\xi}_k^i\mathbf{K}_i, \text{ with } \mathbf{K}_i = \mathbf{G}_i^{-1}\mathbf{F}_i \tag{26}$$

and, replacing the matrices $\mathbf{F}_i$ by $\mathbf{F}$ and $\mathbf{G}_i$ by $\mathbf{G}$ in (23) or (25), the constant gain $\mathbf{K}$ simply by

$$\mathbf{K} = \mathbf{G}^{-1}\mathbf{F}. \tag{27}$$

3.2. Limiting the noise effect

From the thermal system (14) with (15) and (16), the detrimental effect of the measurement noise on the estimated cell temperature and the interest of limiting this effect are illustrated in simulation. Note that, near zero current, the observability matrix is not of full rank so that the system is not observable. Thus for $|I_{bat}| < 0.5A$ (maximum considered sensor error), the observer is not active and only the open loop model (14) is run. Another solution could be to estimate only a part of the states and so to consider a constant internal resistance at low load.

For a battery current switching from 0.5A to 100A at 100s during 100s and a temperature of the air cooling the module $T_{air} = 30°\text{C}$, the observers are simulated when a white Gaussian measurement noise, with a rather weak standard deviation of 0.1°C, is added to the air temperature T_{sens} given by the thermistor. A wide range of variation $0.5\text{A} \leq |I_{bat}| \leq 400\text{A}$ is considered for the charge/discharge current. Since the time varying parameter $\rho_k = I_{bat}^2(k)$ is scalar, the polytopic decomposition (18) reduces to elementary computations. Indeed, ρ_k evolves between the minimal ρ_{min} and maximal ρ_{max} values, which are the $N = 2$ vertices θ_1 and θ_2 of the convex polytope $\mathcal{D}_\rho$. Thus, (18) turns into $\rho_k = \xi_k^1\rho_{min} + \xi_k^2\rho_{max}$. Since $\sum_{i=1}^{N} \xi_k^i = 1$, $\rho_k = \xi_k^1\rho_{min} + (1 - \xi_k^1)\rho_{max}$, and (19) is reduced to $\mathbf{A}(\rho_k) = \xi_k^1\mathbf{A_1} + (1 - \xi_k^1)\mathbf{A_2}$, where $\mathbf{A_1}$ and $\mathbf{A_2}$ are obtained from $\mathbf{A}$ (15) by replacing $I_{bat}^2(k)$ by $\rho_{min} = 0.5^2$ and $\rho_{max} = 400^2$.

By applying Theorem 1 ignoring the measurement noise and solving the LMIs (23) with the toolbox Yalmip[1], a time varying gain observer gain $\mathbf{K}(\boldsymbol{\rho}_k)$ (26) is obtained by linear interpolation between the gains $\mathbf{K_1} = [16.3139\ 1.6241\ -0.0738078\ 0.528547]^T$ and $\mathbf{K_2} = [23.2229\ 1.65147\ -0.0700501\ 0.519493]^T$. Nevertheless, as illustrated in Fig. 5, the observer yields noisy estimates, particularly for T_{cell}.

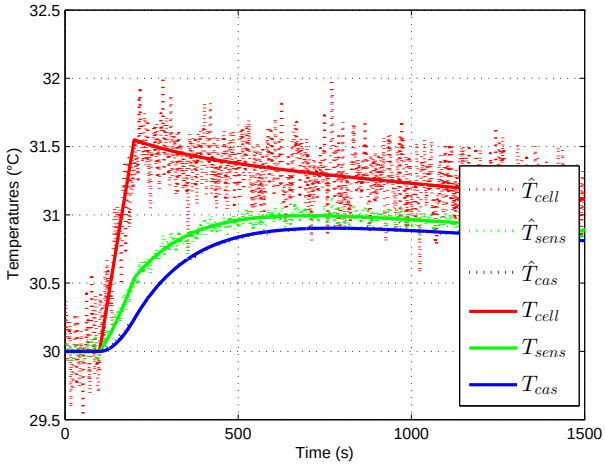

Figure 5: Simulation results with noise using Theorem 1.

By using now Theorem 2 with $\tilde{\mathbf{C}}(1, 1) = 1, \tilde{\mathbf{C}}(i, j) = 0, i, j \neq 1$, in order to limit the noise effect on the reconstruction of

[1] http://users.isy.liu.se/johanl/yalmip

T_{cell}, the gains $\mathbf{K_1}$ and $\mathbf{K_2}$ are found to be similar. Then Theorem 2 is applied to find a constant observer gain (27). Solving the corresponding LMIs with, for (24), $\sigma = 7.8$ then yields $\mathbf{K} = [0.41883\ 0.12281\ 0.03594\ 0.00010075]^T$. The results given in Fig. 6 show that the observer with a constant gain, easier to implement in real time, is suitable for the considered application, and is robust to noise. Recall that the high level bound σ (24) can be tuned in order to decrease the noise effect.

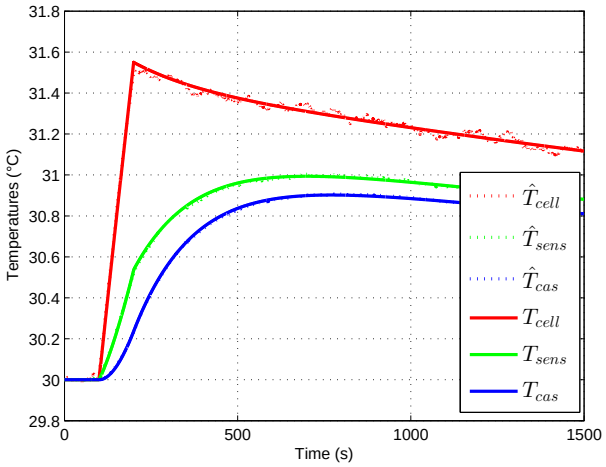

Figure 6: Simulation with noise using Theorem 2 (constant gain, $\sigma = 7.8$).

4. Experimental Results

The observer proposed in Theorem 2, with a constant gain (27), is now applied on two real data sets (a normal use and a battery overcharge) for the reconstruction of the cell temperature and internal resistance, still based on model (14) with (15) and (16).

4.1. Normal use

The first real cycle, shown on Fig. 7, concatenates a typical EV charge depleting and a complete charge of the battery. Note that this State Of Charge (SOC) estimation is not used by the observer, that allows the battery monitoring unit to be independant of this estimated variable. Again, for the state reconstruction, a wide range of variation $0.5\text{A} \leq |I_{bat}| \leq 400\text{A}$ is considered for the charge/discharge current. With $\sigma = 7.8$, a constant observer gain $\mathbf{K} = [0.41883\ 0.12281\ 0.03594\ 0.00010075]^T$ is obtained. Fig. 8 shows that the temperatures T_{sens} and T_{cas} are very well estimated, and that the cell temperature T_{cell} is estimated with a good accuracy, at least sufficient for real time reconstruction and monitoring of the internal battery temperature. The corresponding estimated time varying cell internal resistance is shown in Fig. 9 compared with the estimation

$$\hat{R} = f(T_{sens}, SOC) \tag{28}$$

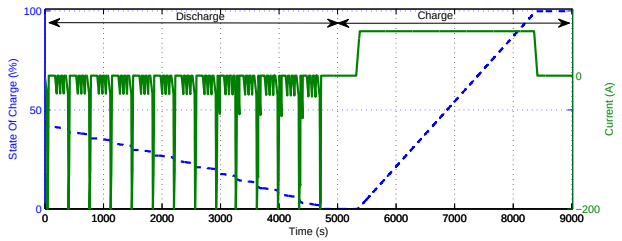

Figure 7: Battery current (A) (solid line) and State Of Charge (%) (dashed line) versus time (s) for the first experimental test.

where f is commonly given by a look-up table. This table is illustrated on Fig. 10 and the estimation $\hat{R}$ is calculated from data shown on Fig. 8 for T_{sens}, and Fig. 7 for SOC. The trends of both the estimations are similar. The differences can be attributed to the fact that the look-up table was built from a cell at the beginning of its life with a static identification of the internal resistance whereas the module used for the observer design of internal cell temperature and resistance was equipped with cells in the middle of their lifecycle. Moreover, the observed internal resistance represents the overall impedance of the cell which is not the same as the static resistance (Jossen, 2006).

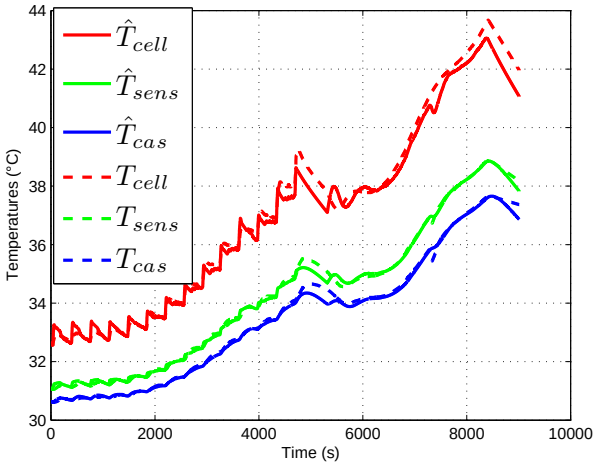

Figure 8: Real and estimated temperatures (constant gain, $\sigma = 7.8$).

Table 2 shows the Root Mean Squared Error and the correlation coefficient for the observation of the three temperatures T_{cell}, T_{sens} and T_{cas} on the validation data of Section 2.3. The observer improves the previous "open loop" estimation shown on Table 1. Note that it gives relevant results even with a reduced thermal model and the assumption of slowly varying internal resistance.

4.2. Overcharge

The observer is now applied in a second real test, a battery overcharge with a constant current of 8A. The real and estimated temperatures are shown on Fig. 11 and the corresponding estimated cell internal resistance on Fig. 12. Because the look-up table does not include overcharge conditions, no comparison

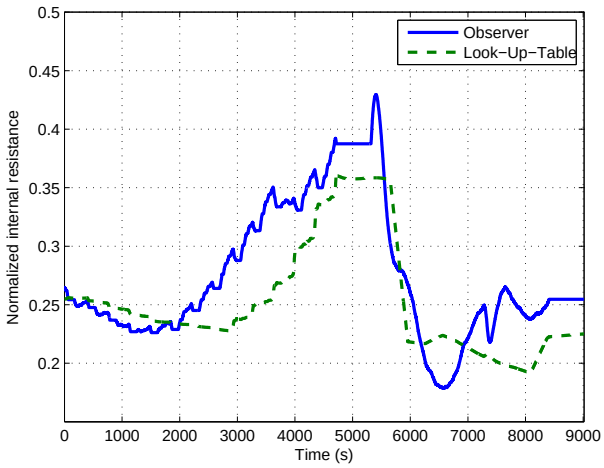

Figure 9: Estimated (normalized w.r.t. minimum and maximum) internal resistances: proposed observer (blue solid line) and look-up-table (28) (green dash line).

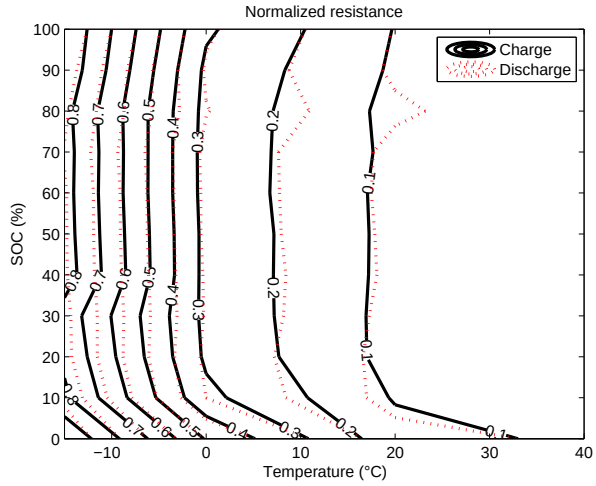

Figure 10: Look-up table of the internal resistance (normalized w.r.t. minimum and maximum) w.r.t. temperature and State Of Charge.

Table 2: Root Mean Squared Error (RMSE) and correlation coefficient with the polytopic observer for the estimation of the three temperatures T_{cell}, T_{sens} and T_{cas} on the validation data.

Temperature	RMSE (°C)	Correlation coef.
T_{cell}	0.38	0.997
T_{sens}	0.14	0.998
T_{cas}	0.14	0.998

is given. However it is known that in the case of overcharge the internal resistance increases (Hall et al., 2005). Hence, the simultaneous reconstruction of the cell temperature and internal resistance makes it possible to detect overcharges by checking a threshold crossing of the estimated resistance. For example, as the resistance is normalized, it must be always less than 1, which is not the case on Fig. 12 due to the overcharge. The proposed overcharge detection from the estimation of internal resistance increases the battery safety since overcharge can be monitored by two independant modules of the Battery Management System (BMS), the standard one using a cell voltage sensor and the proposed one based on current and temperature sensors.

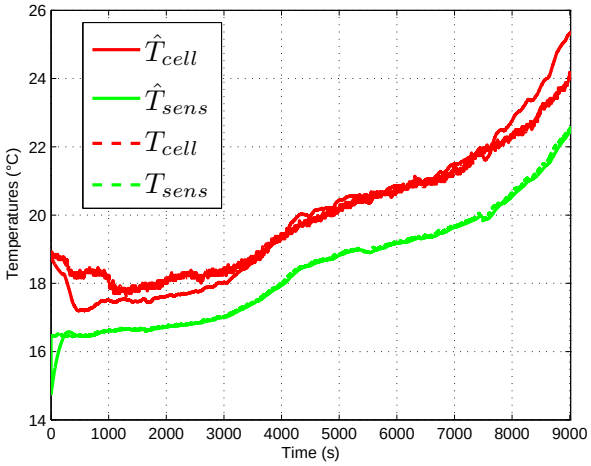

Figure 11: Real and estimated temperatures during a battery overcharge.

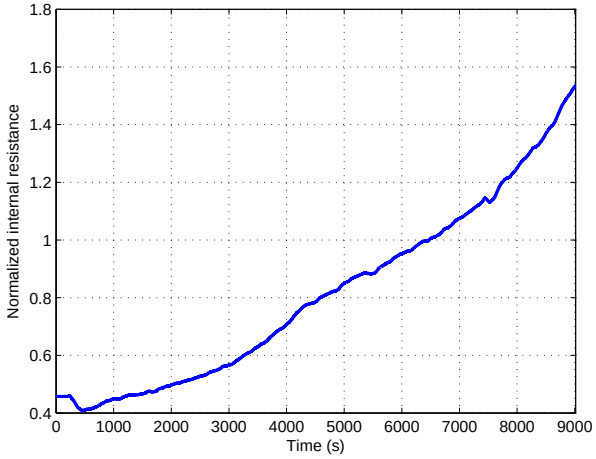

Figure 12: Estimated cell internal resistance (normalized) during a battery overcharge.

5. Conclusion

For the simultaneous estimation of the cell temperature and internal resistance of a Li-ion battery pack, a control-oriented thermal modelling has been carried out. This led to a LPV model from which an observer, with guaranteed convergence, can be designed. A generic approach for LPV systems limiting the influence of measurement noise on the estimates has been proposed. Considering the quality of the estimation which has been demonstrated on real data, the proposed observer could be included in the battery management systems of electric vehicles to increase availability, longevity and safety of the batteries. Indeed, the simultaneous reconstruction of the cell temperature and internal resistance makes it possible to develop diagnosis functions in order for example to detect overcharges increasing the safety during the battery charge procedure.

6. Appendix : Proof of Theorem 2

Proof. Let us define matrices $\mathbb{G}_i$, $\mathbb{P}_i$ et $\mathbb{M}_i$:

$$\mathbb{G}_i = \begin{bmatrix} \mathbf{G}_i & \mathbf{0} \\ \mathbf{0} & \sigma\mathbf{1} \end{bmatrix}, \mathbb{P}_i = \begin{bmatrix} \mathbf{P}_i & \mathbf{0} \\ \mathbf{0} & \sigma\mathbf{1} \end{bmatrix}, \mathbb{M}_i = \begin{bmatrix} \mathbf{A}_i - \mathbf{F}_i\mathbf{C} & -\mathbf{F}_i\mathbf{D} \\ \sigma^{-1}\tilde{\mathbf{C}} & \mathbf{0} \end{bmatrix} \tag{29}$$

Equation (25) can be rewritten as:

$$\begin{bmatrix} \mathbb{P}_i & (\mathbb{G}_i\mathbb{M}_i)^T \\ \mathbb{G}_i\mathbb{M}_i & \mathbb{G}_i + \mathbb{G}_i^T - \mathbb{P}_j \end{bmatrix} > 0. \tag{30}$$

As $\mathbb{P}_i$ is strictly positive, then:

$$\mathbb{G}_i\mathbb{P}_j^{-1}\mathbb{G}_i^T \geq \mathbb{G}_i + \mathbb{G}_i^T - \mathbb{P}_j \tag{31}$$

and thus:

$$\begin{bmatrix} \mathbb{P}_i & (\mathbb{G}_i\mathbb{M}_i)^T \\ \mathbb{G}_i\mathbb{M}_i & \mathbb{G}_i\mathbb{P}_j^{-1}\mathbb{G}_i^T \end{bmatrix} > 0. \tag{32}$$

This inequality is identical to:

$$\begin{bmatrix} \mathbf{1} & \mathbf{0} \\ \mathbf{0} & \mathbb{G}_i\mathbb{P}_j^{-1} \end{bmatrix} \begin{bmatrix} \mathbb{P}_i & \left(\mathbb{P}_j\mathbb{M}_i\right)^T \\ \mathbb{P}_j\mathbb{M}_i & \mathbb{P}_j \end{bmatrix} \begin{bmatrix} \mathbf{1} & \mathbf{0} \\ \mathbf{0} & (\mathbb{G}_i\mathbb{P}_j^{-1})^T \end{bmatrix} > 0 \tag{33}$$

and thus:

$$\begin{bmatrix} \mathbb{P}_i & \left(\mathbb{P}_j\mathbb{M}_i\right)^T \\ \mathbb{P}_j\mathbb{M}_i & \mathbb{P}_j \end{bmatrix} > 0 \tag{34}$$

because $\mathbb{G}_i$ et $\mathbb{P}_j$ are full rank matrices.

Finally, for each $i = 1 \dots N$, the $j = 1 \dots N$ inequalities (34) are multiplied by $\boldsymbol{\xi}_{k+1}^j$ and summed. Then, the $i = 1 \dots N$ inequalities are multiplied by $\boldsymbol{\xi}_k^i$ and summed again. Then:

$$\begin{bmatrix} \mathbb{P}_k & (\mathbb{P}_{k+1}\mathbb{M})^T \\ \mathbb{P}_{k+1}\mathbb{M} & \mathbb{P}_{k+1} \end{bmatrix} > 0 \tag{35}$$

with $\mathcal{P}_k = \sum_{i=1}^N \boldsymbol{\xi}_k^i \mathbf{P}_i$ et $\mathcal{P}_{k+1} = \sum_{i=1}^N \boldsymbol{\xi}_{k+1}^i \mathbf{P}_i$. With the Schur complement, one has directly:

$$\mathbb{M}^T\mathbb{P}_{k+1}\mathbb{M} - \mathbb{P}_k < 0 \tag{36}$$

with

$$\mathbb{P}_{k+1} = \begin{bmatrix} \mathcal{P}_{k+1} & \mathbf{0} \\ \mathbf{0} & \sigma\mathbf{1} \end{bmatrix}, \mathbb{P}_k = \begin{bmatrix} \mathcal{P}_k & \mathbf{0} \\ \mathbf{0} & \sigma\mathbf{1} \end{bmatrix}, \mathbb{M} = \begin{bmatrix} \mathcal{A} & \mathcal{B} \\ \sigma^{-1}\tilde{\mathbf{C}} & \mathbf{0} \end{bmatrix} \tag{37}$$

and finally $\mathcal{A} = \sum_{i=1}^N \boldsymbol{\xi}_k^i (\mathbf{A}_i - \mathbf{F}_i\mathbf{C})$ and $\mathcal{B} = \sum_{i=1}^N \boldsymbol{\xi}_k^i (-\mathbf{F}_i\mathbf{D})$. Equation (36) can be then rewritten as:

$$\begin{bmatrix} \mathcal{A}^T\mathcal{P}_{k+1}\mathcal{A} + \sigma^{-1}\tilde{\mathbf{C}}^T\tilde{\mathbf{C}} - \mathcal{P}_k & \mathcal{A}^T\mathcal{P}_{k+1}\mathcal{B} & \mathbf{0} \\ \mathcal{B}^T\mathcal{P}_{k+1}\mathcal{A} & \mathcal{B}^T\mathcal{P}_{k+1}\mathcal{B} - \sigma\mathbf{1} & \mathbf{0} \\ \mathbf{0} & \mathbf{0} & -\sigma\mathbf{1} \end{bmatrix} < 0. \tag{38}$$

Multiplying, respectively left and right, by $[\boldsymbol{\epsilon}_k \mathbf{v}_k]$ and its transpose, leads to:

$$V(\boldsymbol{\epsilon}_{k+1}, \boldsymbol{\xi}_{k+1}) - V(\boldsymbol{\epsilon}_k, \boldsymbol{\xi}_k) + \sigma^{-1}(\tilde{\mathbf{C}}\boldsymbol{\epsilon}_k)^T(\tilde{\mathbf{C}}\boldsymbol{\epsilon}_k) - \sigma\mathbf{v}_k^T\mathbf{v}_k < 0. \tag{39}$$

Considering this equation for $k = 0 \dots N$ and summing leads to:

$$V(\boldsymbol{\epsilon}_{N+1}, \boldsymbol{\xi}_{N+1}) + \sigma^{-1}\sum_{k=0}^{N}(\tilde{\mathbf{C}}\boldsymbol{\epsilon}_k)^T(\tilde{\mathbf{C}}\boldsymbol{\epsilon}_k) - \sigma\sum_{k=0}^{N}\mathbf{v}_k^T\mathbf{v}_k < 0 \tag{40}$$

. Because $V(\boldsymbol{\epsilon}_{N+1}, \boldsymbol{\xi}_{N+1}) = \boldsymbol{\epsilon}_{N+1}^T\mathcal{P}_k\boldsymbol{\epsilon}_{N+1} > 0$, then :

$$\sigma^{-1}\sum_{k=0}^{N}(\tilde{\mathbf{C}}\boldsymbol{\epsilon}_k)^T(\tilde{\mathbf{C}}\boldsymbol{\epsilon}_k) < \sigma\sum_{k=0}^{N}\mathbf{v}_k^T\mathbf{v}_k \tag{41}$$

and, when $N \to \infty$, this expression is equivalent to (24).

□

Broussely, M., Biensan, P., Bonhomme, F., Blanchard, P., Herreyre, S., Nechev, K., Staniewicz, R., 2005. Main aging mechanisms in Li ion batteries. Journal of Power Sources 146 (1-2), 90–96.

Cheron, B., 1999. Transferts thermiques. Ellipses.

Debert, M., Colin, G., Mensler, M., Chamaillard, Y., Guzzella, L., 2008. Li-ion battery models for HEV simulator. In: IFP (Ed.), Advances in hybrid powertrains. Rueil-Malmaison, France.

Forgez, C., Do, D. V., Friedrich, G., Morcrette, M., Delacourt, C., 2010. Thermal modeling of a cylindrical $LiFePO_4$/graphite lithium-ion battery. Journal of Power Sources 195 (9), 2961–2968.

Guzzella, L., Sciarretta, A., 2007. Vehicle Propulsion Systems. Introduction to Modeling and Optimization, 2nd Edition. Springer.

Halimi, M., Millérioux, G., Daafouz, J., 2013. Polytopic observers for LPV discrete-time systems. In: Robust Control and Linear Parameter Varying Approaches. Vol. 437 of Lecture Notes in Control and Information Sciences. pp. 97–124.

Hall, J., Schoen, A., Powers, A., Liu, P., Kirby, K., 2005. Resistance growth in lithium ion satellite cells. I. Non destructive data analyses. In: 208th Electrochemical Society Meeting. Los Angeles, CA, October 16-21.

Hu, Y., Yurkovich, S., 2012. Battery cell state-of-charge estimation using linear parameter varying system techniques. Journal of Power Sources 198, 338–350.

Hu, Y., Yurkovich, S., Guezennec, Y., Yurkovich, B. J., 2009. A technique for dynamic battery model identification in automotive applications using linear parameter varying structures. Control Engineering Practice 17 (10), 1190–1201.

Jossen, A., 2006. Fundamentals of battery dynamics. Journal of Power Sources 154 (2), 530–538.

Lin, X., Perez, H. E., Siegel, J. B., Stefanopoulou, A. G., Li, Y., Anderson, R. D., Ding, Y., Castanier, M. P., 2013. Online parameterization of lumped thermal dynamics in cylindrical lithium ion batteries for core temperature estimation and health monitoring. IEEE Transactions on Control System Technology, to appear.

Lin, X., Stefanopoulou, A. G., Perez, H. E., Siegel, J. B., Li, Y., Anderson, R. D., 2012. Quadruple adaptive observer of the core temperature in cylindrical li-ion batteries and their health monitoring. In: Proc. American Control Conference. Montréal, QC, Canada, pp. 578–583.

Millérioux, G., Anstett, F., Bloch, G., 2005. Considering the attractor structure of chaotic maps for observer-based synchronization problems. Mathematics and Computers in Simulation 68 (2), 67–85.

Millérioux, G., Daafouz, J., 2006. Performances of unknown input observers for chaotic LPV maps in a stochastic context. Nonlinear Dynamics 44, 205–212.

Millérioux, G., Rosier, L., Bloch, G., Daafouz, J., 2004. Bounded state reconstruction error for LPV systems with estimated parameters. IEEE Transactions on Automatic Control 49 (8), 1385–1389.

Muratori, M., Canova, M., Guezennec, Y., Rizzoni, G., 2010. A reduced-order model for the thermal dynamics of Li-ion battery cells. In: 6th IFAC Symposium Advances in Automotive Control. Munich, Germany.

Pesaran, A. A., 2002. Battery thermal models for hybrid vehicle simulations. Journal of Power Sources 110 (2), 377–382.

Plett, G. L., 2004. Extended Kalman filtering for battery management systems of LiPB-based HEV battery packs: Part 3. State and parameter estimation. Journal of Power Sources 134 (2), 277–292.

Ratnakumar, B. V., Smart, M. C., Blosiu, J. O., Surampudi, S., 1999. Storage characteristics of Lithium ion cells. In: Lithium Batteries, Electrochemical Society Proceedings. Vol. 99-25. pp. 706–718.

Vetter, J., Novak, P., Wagner, M. R., Veit, C., Möller, K.-C., Besenhard, J. O., Winter, M., Wohlfart-Mehrens, M., Vogler, C., Hammouche, A., 2005. Ageing mechanisms in lithium-ion batteries. Journal of Power Sources 147 (1-2), 269–281.

Williford, R. E., Viswanathan, V. V., Zhang, J.-G., 2009. Effects of entropy changes in anodes and cathodes on the thermal behavior of lithium ion batteries. Journal of Power Sources 189 (1), 101–107.